The importance of ocean transport in the fate of anthropogenic CO_2

L. Cao[1*], M. Eby[2], A. Ridgwell[3], K. Caldeira[1], D. Archer[4], A. Ishida[5], F. Joos[6], K. Matsumoto[7], U. Mikolajewicz[8], A. Mouchet[9], J. C. Orr[10], G.-K. Plattner[6,14], R. Schlitzer[11], K. Tokos[7], I. Totterdell[12,15], T. Tschumi[6], Y. Yamanaka[13], A. Yool[12]

[1] Department of global ecology, Carnegie Institution, Stanford, California, USA

[2] School of Earth and Ocean Sciences, University of Victoria, Victoria, British Columbia, Canada

[3] School of Geographical Sciences, University of Bristol, Bristol, United Kingdom

[4]Department of the Geophysical Sciences, University of Chicago, Chicago, IL, USA

[5] Frontier Research Center for Global Change, Japan Agency for Marine-Earth Science and Technology, Yokohama, Japan

[6] Climate and Environmental Physics, Physics Institute and Oeschger Centre for Climate Change Research, University of Bern, Bern, Switzerland

[7] Department of Geology and Geophysics, University of Minnesota, Minneapolis, USA

[8]Max Planck Institute for Meteorology, Bundesstrasse 53, 20146 Hamburg, Germany

[9] Department of Astrophysics, Geophysics and Oceanography, University of Liege, Liege, Belgium

[10] Marine Environment Laboratories, International Atomic Energy Agency, Monaco

[11] Alfred Wegener Institute, Bremerhaven, Germany

[12] National Oceanography Centre, Southampton, United Kingdom

[13] Graduate School of Environmental Earth Science, Hokkaido University, Sapporo, Japan

[14] Institute of Biogeochemistry and Pollutant Dynamics, ETH Zürich, Universitätstr., Zürich, Switzerland

[15] Met Office Hadley Centre, Exeter, United Kingdom

* Corresponding author: Long Cao, longcao@stanford.edu

Abstract

We assess uncertainties in projected oceanic uptake of anthropogenic CO_2 associated with uncertainties in model ocean transport using a suite of climate/carbon-cycle models. In response to a CO_2 pulse emission of 590 PgC (corresponding to an instantaneous doubling of atmospheric CO_2 from 278 to 556 ppm), the fraction of CO_2 emitted absorbed by the ocean (model mean ± 2σ) is 37 ± 8 %, 56 ± 10 %, and 81 ± 4 % in year 30, 100, and 1000 after the emission pulse, respectively. Modeled oceanic uptake of excess CO_2 on timescales from decades to about a century is strongly correlated with simulated present-day uptake of chlorofluorocarbons (CFCs) and anthropogenic CO_2, while the amount of excess CO_2 absorbed by the ocean from a century to a millennium is strongly correlated with modeled radiocarbon in the deep Southern and Pacific Ocean. The rates of surface-to-deep ocean transport are determined for individual models from the instantaneous doubling CO_2 experiments, and they are used to calculate oceanic uptake of CO_2 in response to emission pulses of 1000 and 5000 PgC. These results are compared with simulated oceanic uptake of CO_2 from a number of model runs with the coupling of climate-ocean carbon cycle and without it. This comparison demonstrates that the impact of different ocean transport across models on the oceanic uptake of anthropogenic CO_2 is of similar magnitude as that of climate-carbon cycle feedbacks in a single model associated with changes in temperature, circulation, and marine biology, emphasizing the importance of ocean transport in the fate of anthropogenic CO_2.

1 Introduction

Atmospheric CO_2 is expected to increase in the near future due to continued emissions from fossil fuel burning and land use changes. A major uncertainty in projecting future climate change is how much this emitted CO_2 will remain in the atmosphere. Different processes acting on different timescales are responsible for the removal of excess CO_2 from the atmosphere. For example, the present ocean is, and the terrestrial biosphere appears to be, a net sink for anthropogenic carbon (Denman et al., 2007). Over the coming decades to centuries, the ocean is expected to continue acting as a CO_2 sink while the land could change from a net carbon sink to source (e.g., Cox et al., 2000; Bala et al., 2005). On timescales of a millennium and beyond, the reaction of dissolved CO_2 with calcium carbonate ($CaCO_3$) in deep ocean sediments will start to play an important role in buffering the human carbon perturbation (Broecker and Takahashi, 1978; Archer 1997). On timescales of several hundred thousands of years the still airborne anthropogenic CO_2 will be removed from the atmosphere by the weathering of silicate rocks (Walker and Kasting, 1992; Zeebe and Caldeira, 2008).

An accurate projection of the oceanic uptake of anthropogenic CO_2 is important. On one hand, the amount of anthropogenic CO_2 absorbed by the ocean affects atmospheric CO_2 concentrations. The airborne anthropogenic CO_2 on millennial timescale, which is primarily determined by oceanic uptake of human-emitted carbon, has great implications for future sea level rise and ice sheet extent (Archer, 2005). On the other hand, oceanic uptake of anthropogenic CO_2 modifies ocean chemistry by making it more acidic, an urgent environmental problem independent of global warming (Caldeira and Wickett, 2003; Orr et al., 2005; Royal Society, 2005; Cao et al., 2007; Cao and Caldeira, 2008; Steinacher et al., submitted).

87 Global carbon cycle models are used to project the ability of the ocean and terrestrial biosphere
88 to take up anthropogenic CO_2, but projections of CO_2 uptake differ widely between models and
89 on different timescales. Simulated carbon uptake in the 1990s by models participating in the
90 Ocean Carbon Model Intercomparison Project (OCMIP-2) varies between 1.98 and 3.04 PgC (1
91 PgC $=10^{15}$ g carbon) when atmospheric CO_2 was prescribed according to the IPCC S650 CO_2
92 stabilization scenario (Orr et al., 2002). Accumulated oceanic carbon uptake at the time of
93 doubling CO_2 varies by a factor of two across eleven 3-D coupled carbon cycle/climate models
94 participating in the Coupled Climate-Carbon Cycle Intercomparison Project (C4MIP) and forced
95 with IPCC SRES A2 emission scenario (Friedlingstein et al., 2006). The fraction of CO_2
96 absorbed by the ocean ranges from 24 to 34% in year 2100 and 49 to 62% in year 3000 for eight
97 Earth system models forced by a scenario in which total CO_2 emission reaches about 1600 PgC
98 by year 2100 and is kept constant thereafter (Plattner et al., 2008). Regarding the long-term fate
99 of anthropogenic CO_2, model-projected airborne fraction ranges from 35 to 58% and 23 to 47%
100 1000 and 5000 years from now in response to a CO_2 emission pulse of about 5000 PgC (Archer,
101 2005; Lenton and Britton, 2006; Ridgwell and Hargreaves, 2007, Montenegro et al., 2007). A
102 recent model intercomparison study shows that in response to a CO_2 emission pulse of 5000 PgC,
103 model-projected airborne CO_2 ranges between 20 and 30% 10,000 years after the emission pulse
104 (Archer et al., submitted).
105
106 The discrepancy in projected atmospheric CO_2 and/or anthropogenic CO_2 uptake by the ocean
107 across models can be attributed to differences in model representations of various processes,
108 including ocean transport, biological uptake by both the ocean and terrestrial biosphere,
109 sedimentation of calcium carbonate, and their interactions with climate change. Of these

processes, ocean transport is a key player. First, the rate of ocean transport determines the rate by which anthropogenic CO_2 is transferred from the surface to the deep ocean. Second, on timescales over a millennium, the rate of ocean transport determines the rate by which anthropogenic CO_2 reaches ocean sediments and carbonate ions released from dissolving $CaCO_3$ returns to the surface and further neutralize fossil fuel CO_2. Therefore, ocean transport also affects the timescale of "$CaCO_3$ neutralization" (e.g., Archer et al., 1997; Ridgwell and Hargreaves, 2007). Third, ocean transport affects biological CO_2 uptake by controlling the availability of nutrients at ocean surface and the export of organic matter from surface waters to the deep ocean.

The purpose of this paper is to assess the effect of ocean transport on the uptake of anthropogenic CO_2 by comparing simulation results from a number of models. The models used in this study and experimental protocols are introduced in the next section. Model responses to different CO_2 emission pulses are presented in section 3. We first investigate modeled ocean responses to a pulse release of 2 times CO_2 and discuss how they are related to simulated inventories of chemical tracers such as radiocarbon and Chlorofluorocarbons (CFCs). We then present surface ocean response functions that characterize the rate of ocean transport for individual models, and use them to determine CO_2 uptake in response to emission pulses of 1000 and 5000 PgC. The impact of ocean transport on oceanic CO_2 uptake is compared to that of climate change feedbacks. Discussion and conclusions follow in section 4.

2. Models and experiment protocols

A suite of climate/carbon-cycle models of different complexities are used in this study. These include three models derived from the Grid ENabled Integrated Earth system model (GENIE-1,

Edwards and Marsh, 2005): GENIE8 (8 ocean levels, Ridgwell et al., 2007a); GENIE16 (16 ocean levels, Singarayer et al., 2008); and MESMO (16 ocean levels, Matsumoto et al., 2008) (In addition to vertical resolution, these three versions of GENIE-1 differ in other aspects), the University of Victoria Earth System Climate Model (UVic, Weaver et al., 2001), Bern3D ocean model (Müller et al., 2006) with its physical core modified from Edwards et al. (1998) and Edwards and Marsch (2005), MPI-UW Earth system model (Mikolajewicz et al., 2007), high-latitude exchange/interior diffusion-advection (HILDA) model (Siegenthaler and Joos, 1992), and a modified HILDA model, LTCM (stands for the Long-term Carbon Cycle Model). In addition, archived results from five ocean carbon cycle models (AWI, Bern2.5D (previously known as PIUB), IGCR, SOC, UL) participating in phase II of the Ocean Carbon-Cycle Model Intercomaprison Project (OCMIP-2) and performing CO_2 pulse emission experiments (http://www.ipsl.jussieu.fr/OCMIP/) are investigated. The ocean component of these models are all coarse-resolution, non-eddy-resolving models, but they differ considerably in their configurations including the grid resolution, sub-grid scale mixing parameterizations, and surface forcing. The main characteristics of each model are listed in Table 1, and details of these models are given in appendix A.

Carbon uptake experiments in response to an instantaneous CO_2 emission pulse were performed following the OCMIP-2 protocol(http://www.ipsl.jussieu.fr/OCMIP/phase2/simulations/Abiotic/HOWTO-Abiotic.html). Starting from the model pre-industrial state a CO_2 emission pulse of 590.2 PgC (corresponding to an instantaneously doubling of atmospheric CO_2 concentration from 278 to 556 ppm by applying the conversion factor of 1 ppm = 2.123 PgC as used in OCMIP) is added to each model, and then atmospheric CO_2 is determined by air-sea exchange. The entire integration lasted for 1000 years. To have a direct comparison with OCMIP-2 simulations,

processes other than the ocean carbon cycle, including CO_2 uptake by the terrestrial biosphere, interaction with $CaCO_3$ sediment, and climate change feedbacks are disabled in the CO_2 pulse emission experiments. To evaluate modeled oceanic uptake of CO_2 against their skills in simulating chemical tracers, simulations of natural radiocarbon (in terms of $\Delta^{14}C$) and historical uptake of anthropogenic CO_2 and CFCs were also performed.

3. Results

3.1 Double CO_2 experiments

Time series of modeled oceanic uptake in response to an instantaneous CO_2 emission of 590 PgC are shown in Fig. 1. Among the models shown here, UL has the largest oceanic uptake, while UVic and GENIE16 have the lowest. The fraction of the total CO_2 emission absorbed by the ocean varies from 34 to 45 %, 50 to 65 %, and 77 to 84 %, with a cross model mean (±1 standard deviation, 1σ) of 37 ± 4 %, 56 ± 5 %, and 81 ± 2 % in year 30, 100, and 1000 after the emission pulse, respectively. Many models have not reached steady state 1000 years after the emission pulse (in the absence of sediment $CaCO_3$ neutralization). For example, the fraction of oceanic uptake of excess CO_2 by Bern3D and LTCM is 80.7% and 82.2% in year 1000, which increases to 82.6% and 83.3% in year 2000 when the model has reached steady-state.

Many factors could contribute to the difference in oceanic uptake of CO_2 across models, such as parameterization schemes of ocean mixing and surface boundary forcing (see Table 1). An extensive exploration of the role for each factor is beyond the scope of this study. Nonetheless, sensitivity experiments using GENIE16 show that differences in the intensity of vertical mixing, model vertical resolutions, and representation of the seasonal cycle all responsible for part of the

discrepancies in modeled oceanic CO_2 uptake (Fig. S1).One caveat is that the OCMIP model results presented here were from abiotic runs, while other model simulations include a component of marine biology. However, as long as the strength of biological carbon transport remains unchanged, as in the double CO_2 experiments where no feedbacks from changes in climate and biology are included, marine biology plays a minor role in the uptake of anthropogenic CO_2. This is shown by our sensitivity experiments (Fig. S2) and also found by previous studies (Maier-Reimer, 1993; Murnane et al., 1999).

Positive correlations are observed between modeled CO_2 uptake and the uptake/inventories of different tracers that characterize the rate of ocean transport on different timescales (Fig. 2, 3, 4). On the decadal timescale, modeled oceanic uptake of CO_2 in response to doubling CO_2 pulse is strongly correlated with present-day uptake of both CFC11 and anthropogenic CO_2. Beyond a century, the correlation with the uptake of CFC11 becomes weaker while strong correlation with the uptake of anthropogenic CO_2 (with r greater than 0.7) extends to a few centuries. These observations are consistent with the fact that the uptake of anthropogenic CO_2 during the past is characterized by an ocean ventilation timescale of a few centuries, while the uptake of CFCs is characterized by an ocean ventilation timescale of several decades. On timescales from a century to a millennium, the amount of CO_2 absorbed by the ocean is strongly correlated with the content of natural radiocarbon in the deep ocean, which is governed by ocean ventilation over hundreds to thousands of years. This correlation is particularly strong with radiocarbon in the deep Southern (with r greater than 0.8) and Pacific Ocean (with r greater than 0.7), indicating that the processes controlling ventilation of the deep Southern and Pacific Ocean have a strong control on the long-term efficiency of oceanic uptake for anthropogenic CO_2.

198 3.2 Surface ocean response functions

199 One key player in the oceanic uptake of anthropogenic CO_2 is the rate of surface-to-deep ocean
200 transport. However, the role of ocean transport is obscured by the influences from other factors,
201 such as buffering capacity of the carbonate system and the rate of air-sea gas exchange. To
202 separate the effect of ocean transport from other factors, we adopt the method of Joos et al. (1996)
203 to determine surface ocean pulse response functions that characterize the rate of surface-to-deep
204 ocean transport. The theoretical justification of the ocean pulse response functions is that the
205 dynamics of a linear system can be fully characterized by its pulse (or Green's) function, and the
206 transport of tracers in the ocean is described by a set of linear equations under steady state
207 (constant circulation). Atmospheric and/or surface ocean pulse response functions have therefore
208 been used to compare the uptake characteristics of anthropogenic carbon by ocean transport
209 models (Maier-Reimer and Hasselmann, 1987, Sarmiento et al., 1992, Joos et al., 1996) and to
210 build cost-efficient substitutes of more complex models for the uptake of carbon, heat and other
211 tracers (Joos and Bruno, 1996). Compared to the atmospheric pulse response functions, the use
212 of surface ocean pulse response functions avoids the problem arising from nonlinearities of the
213 carbon chemistry and gives therefore more accurate results.

214 The use of surface ocean response functions is based on the reasoning that surface concentration
215 of dissolved inorganic carbon (DIC_s) at a certain time t can be represented by the convolution
216 integral of earlier carbon input, i.e. the air-sea carbon flux (f_{as}) at time t', multiplied by the
217 fraction of the flux that is still found in the surface layer after time t-t' (ocean surface response,
218 r_s). This can be represented by the following equation (from equation 2 of Joos et al., 1996)

$$DIC_s(t) = \frac{1}{h}\int_{t0}^{t} f_{as}(t^{'}) r_s(t-t')dt' + DIC_s(t_0)$$

where h is model top layer thickness and t_0 is the time at which surface ocean is in equilibrium with the deep ocean. Given surface carbon concentration (DIC_s) and air-sea carbon flux (f_{as}), the ocean surface response (r_s) can be solved from the above equation.

Surface ocean response functions were derived for a subset of models using the above equation and globally averaged output of surface DIC and air-sea flux from 590 PgC CO_2 pulse emission experiments. The results are shown in Fig.5a. These responses represent the fraction of excess carbon added to the surface ocean that is still found in the ocean surface after a certain time, and therefore is a measure of the rate by which tracers (CO_2 here) are transported from the surface to the deep ocean. A validation of the derived surface ocean response functions is given in Appendix B.

It is not appropriate to compare surface ocean response functions as shown in Fig.5a directly with each other because models have different surface layer depths (Table 1). Different surface layer depths cause different response functions. For example, the equilibrium responses are mainly determined by the volume ratios between surface and deep ocean in individual models. To compare the model behavior directly, we normalize the derived ocean surface responses to a uniform surface ocean depth of 50 m, and the differences in the normalized ocean surface response functions represent primarily differences in the rate of surface-to-deep transport between models (Fig 5b). The comparison of Fig.5b with Fig. 1 indicates that models with faster transport from the surface to the deep ocean (lower values of ocean surface response) generally

239 have larger CO_2 uptake by the ocean, suggesting that different ocean transport are mainly
240 responsible for differences in simulated carbon uptake as shown in Fig. 1.

241 3.3 Effect of ocean transport and climate change on anthropogenic CO_2 uptake

242 We investigate to what extent differences in ocean transport across models affect modeled
243 anthropogenic CO_2 uptake by the ocean. Emission scenarios considered here include CO_2
244 emission pulses of 1000 and 5000 PgC. A total CO_2 pulse size of 1000 PgC corresponds to the
245 cumulative CO_2 emissions by the end of the century from some of the comparably modest IPCC
246 scenarios (For example, IPCC SRES A1T scenario has a cumulative CO_2 emission of 1038 PgC
247 from 1990 to 2100), while the 5000 PgC release is roughly equivalent to the amount of available
248 conventional fossil fuel resource (IPCC 2001). To examine the role of ocean transport in
249 anthropogenic CO_2 uptake, we constructed a surface ocean response model following Joos et al.
250 (1996). Input to the surface ocean response model are: a surface ocean depth of 50 m, an ocean
251 area of 3.61×10^{14} m^2, a global mean air-sea exchange rate of 0.061 mol m^{-2} yr^{-1} ppm^{-1} (Broecker
252 et al., 1986), a cubic fit between surface DIC concentrations and ocean surface pCO_2 (to
253 represent buffering capacity of the carbonate system) derived from results of GENIE16
254 simulations, and normalized surface response functions for each model as shown in Fig. 5b. In
255 this way, differences in modeled response to pulse CO_2 emissions are caused only by different
256 rates of ocean transport across models.

257
258 To compare the effect of ocean transport on CO_2 uptake with that of feedbacks from climate
259 change, oceanic CO_2 uptake experiments in response to 1000 and 5000 PgC CO_2 emission pulses
260 were performed by a suite of climate/carbon-cycle models, including UVic, GENIE8, GENIE16,
261 MESMO, HILDA, and MPI-UW used in the 590 PgC emission pulse experiment and two

additional models, CC_SED (Archer 2005) and CLIMBER-2 (Brovkin et al., 2007). These model results were also reported in a recent model intercomparison study for long-term fate of fossil fuel CO_2 (Archer et al., submitted). For each emission scenario, each model was run twice: one with the coupling between climate change and the ocean carbon cycle and the other without it. In this way, the impact of climate change on the ocean carbon cycle was isolated. Since our emphasis in this study is on oceanic uptake of anthropogenic CO_2, processes other than ocean invasion, including uptake by the terrestrial biosphere and deep sea $CaCO_3$ sediment, were disabled in these model runs.

The rate of ocean transport affects physical uptake of anthropogenic CO_2 from the ocean surface to the deep ocean, while climate change affects the physical, chemical, and biological uptake of anthropogenic CO_2 through changes in temperature, circulation, and marine biology. As shown in Fig. 6, the effect of climate change in all models is to decrease oceanic uptake of anthropogenic CO_2 (increase atmospheric CO_2 concentrations by assuming a neutral terrestrial biosphere), but the magnitude of climate change effect varies widely between models. This discrepancy could be attributed to modeled differences in changes to temperature, circulation, and marine biology, and their interactions with the ocean carbon cycle, which merits further investigation.

It is noted that the absolute values of atmospheric CO_2 concentrations calculated from surface ocean response model runs depend on the choices of parameters used in the calculations (e.g., ocean area, air-sea exchange rate, buffering capacity of the carbonate system), but differences between model runs are much less sensitive to input parameters. What we are interested here is not the absolute values of projected atmospheric CO_2, but the difference in projected CO_2

286 concentrations as a result of different ocean transport across models, compared to that as a result
287 of climate feedback on the ocean carbon cycle in a single model. Fig. 6 shows that these two
288 differences are of similar magnitudes, suggesting that the effect of different ocean transport
289 across models on projected atmospheric CO_2 concentrations is comparable to that of climate
290 change in a single model (by assuming a neutral terrestrial biosphere). For example, 100 years
291 after CO_2 emission pulse of 5000 PgC the range of difference in projected CO_2 concentration
292 caused by different ocean transport is 231 ppm, compared with a maximum difference of 165
293 ppm as a result of climate change feedback simulated by MPI-UW. At the same time, the spread
294 of projected CO_2 concentrations due to differences in ocean transport across models is 88 (one
295 standard deviation, 1σ) and 176 (2σ) ppm, compared with the difference of 108 ± 51 ppm (mean
296 ± 1σ) associated with climate change feedbacks in a single model. 1000 years after CO_2 emission
297 pulse of 5000 PgC, the range of difference in projected CO_2 concentration as a result of transport
298 difference is 351 ppm, compared with the maximum climate change effect of 404 ppm simulated
299 by UVic. Meanwhile, the spread of projected CO_2 concentrations due to differences in ocean
300 transport across models is 119 (1σ) and 238 (2σ) ppm, compared with the difference of 228 ± 93
301 (mean ± 1σ) associated with climate change feedbacks in a single model.
302
303 **4. Discussion and conclusions**

304 In the study of oceanic uptake of anthropogenic CO_2, there has been a history of investigation in
305 the effect of climate change on the ocean carbon cycle (e.g., Maier-Reimer et al., 1996;
306 Sarmiento et al., 1998; Joos et al., 1999; Plattner et al., 2001; Chuck et al., 2005; Friedlingstein
307 et al., 2006; Zickfeld, 2007; Plattner et al., 2008), and recently on the potential effects of ocean
308 acidification (e.g., Heinze, 2004, Ridgwell et al., 2007a, Riebesell et al., 2007). It is found here

309 that in the projection of anthropogenic CO_2 uptake by the ocean, the effect of differences in
310 steady state ocean transport across models is of similar magnitude as that of climate feedbacks
311 associated with changes in temperature, circulation, and marine biology (Fig. 6). Our study
312 demonstrates that in the efforts aiming to achieve a more reliable projection of anthropogenic
313 CO_2 uptake by the ocean, to reduce the uncertainty in the simulation of ocean transport is as
314 important as to reduce the uncertainty in the projection of feedback effects on the ocean carbon
315 cycle associated with changes in climate and marine biology. The importance of ocean transport
316 in oceanic CO_2 uptake, as compared with climate change feedbacks, was also found through
317 sensitivity experiments by varying the values of vertical diffusivity and climate sensitivity in a
318 single model (Joos et al., 1999; Plattner et al., 2001).

319 Here we looked at oceanic uptake of anthropogenic CO_2 up to timescales of a millennium and
320 did not include the buffering effect from deep ocean calcium carbonate sediment. On longer
321 timescales, interactions between anthropogenic CO_2 and deep ocean sediment become more
322 important. The rate of ocean transport affects the timescale of $CaCO_3$ neutralization by
323 determining how long it will take the anthropogenic CO_2 absorbed at the ocean surface to reach
324 the sea floor and how long it will take the released carbonate ions from dissolving sedimentary
325 $CaCO_3$ to return to the ocean surface and further neutralize fossil fuel CO_2. Therefore,
326 differences in ocean transport might explain a substantial part of the discrepancies between
327 simulated long-term evolutions of anthropogenic CO_2 (e.g., Archer, 2005; Lenton and Britton,
328 2006; Ridgwell and Hargreaves, 2007, Montenegro et al., 2007, Archer et al., submitted).

329
330 The high sensitivity of modeled oceanic uptake of anthropogenic CO_2 to the simulation of
331 circulation metrics such as radiocarbon suggests that the simulation of these tracers can be used

as metrics for modeled oceanic CO_2 uptake in the future. For example, when model-simulated natural radiocarbon in the deep Southern Ocean is evaluated against observational-based estimates (Fig. 3), OCMIP models presented here and GENIE8 would appear to overestimate the amount of CO_2 taken up by the ocean on timescales from a few centuries to a millennium.

In summary, this study emphasizes the importance of a realistic simulation for ocean transport in the projection of anthropogenic CO_2 uptake by the ocean. In addition to uptake of anthropogenic CO_2, a realistic ocean transport is also important in determining extra heat absorbed by the ocean that is particularly important for the long-term commitment of climate change. Previous studies emphasized the importance of underlying ocean transport and dynamics in the modeling of present-day ocean carbon cycle and associated biological processes (Doney et al., 2004, Najjar et al., 2007). This study further demonstrates that to have a reliable projection of oceanic uptake of anthropogenic CO_2, it is important to better evaluate and improve model's representation of ocean dynamics. This can be achieved by the simulation of a variety of physical and biogeochemical tracers that hold complementary information about the relevant ocean transport processes on a range of timescales (Maier-Reimer, 1993; Marchal et al., 1998; Doney 1999; Matsumoto et al., 2004; Müller et al., 2006, Najjar et al., 2007; Cao and Jain, 2008).

Appendix A: Model description

OCMIP Models

A detailed description of models participating in the OCMIP-2 CO_2 pulse emission experiments (AWI, Bern2.5D, IGCR, SOC, UL) can be found in Orr et al. (2002). A brief description of each OCMIP model presented in this study is given here.

AWI

The AWI model used in this study follows the approach of ocean circulation model of Schlitzer (1995). It has recently been extended to include biogeochemical nutrients and carbon cycles (Schlitzer, 2002). Unlike dynamical models that use approximations to the momentum equation and external forcing at the sea-surface to calculate the time-varying ocean circulation by applying a time-stepping procedure, the AWI model has a steady 3-D flow field representing the steady-state, annual mean circulation of the ocean.

Bern2.5D

Bern2.5D is a physical-biogeochemical climate model that consists of a zonally averaged ocean model (Wright and Stocker, 1992; Wright and Stocker, 1998), coupled to an atmospheric energy balance model (Stocker et al., 1992). The model includes a basic representations of the carbon cycle, both marine (Marchal et al., 1998) and terrestrial (Siegenthaler and Oeschger, 1987) components. The marine biological model is based on the classical Redfield approach and phosphate is used as a limiting nutrient for biological production.

IGCR

The IGCR model was developed based on the ocean physical/biogeochemical model used in Yamanaka and Tajika (1996) for the study on the vertical fluxes of particulate organic matter and

376 calcite. The physical variables are given by the general circulation model with the same finite
377 differential scheme as the GFDL model.

378 **SOC**

379 The model used by the SOC group is the ocean component of the coupled ocean-atmosphere
380 model developed by the Hadley Centre for Climate Research and Prediction, part of the U.K.
381 Meteorological Office. The version of the Hadley Centre model used for the GOSAC simulations
382 is HadCM3L, a coarse resolution form of the HadCM3 model (Gordon et al., 2000).

383 **UL**

384 The UL model results from the CLIO (Coupled Large-scale model, Goosse, 1998) coupled with
385 a comprehensive and prognostic ocean carbon model LOCH (Mouchet and Francois, 1996).

386 **Bern3D**

387 The Bern3D model (Müller et al., 2006) is a cost-efficient, seasonally forced three-dimensional
388 frictional geostrophic balance ocean model. Its physical core is based on the work by Edwards et
389 al (1998) and Edwards and Marsh (2005) and has been modified to feature distinct coefficients
390 for isopycnal diffusion and Gent-McWilliams transport parameterizations, 32 depth layers, and
391 an implicit numerical scheme for vertical diffusion. The transport parameters have been tuned
392 toward observed chlorofluorocarbon inventories and deep ocean radiocarbon signatures. Sea
393 surface temperatures are constrained by restoring and sea surface salinities by flux boundary
394 conditions. An additional anomalous uniform freshwater surface flux of 0.15 Sv from the
395 Atlantic to the Pacific basin is applied in order to intensify and deepen the Atlantic meridional
396 overturning circulation. Forcing fields for wind stress are derived from the NCEP data. The
397 implementation of biogeochemical cycling in the Bern3D model closely follows the OCMIP-2

398 protocols. However, prognostic formulations are applied to compute the production of organic
399 matter, $CaCO_3$, and opal shells (Parekh et al., 2008, Tschumi et al., 2008).

400 **CC_SED**

401 CC_SED was described by Archer (2005). It uses the HAMOCC2 stationary annual mean flow
402 to transport geochemical tracers. The temperature of the ocean is offset uniformly with a 1000-
403 year response time, relaxing to a target temperature determined by a deep-ocean climate
404 sensitivity of 3°C. It is coupled to a sediment model (Archer 1996) and weathering feedbacks are
405 also included (Berner and Kothavala, 2001).

406 **CLIMBR-2**

407 CLIMBER-2 consists of a two-dimensional atmosphere and a two-dimensional multi-basin
408 dynamic ocean. The climate model is coupled to a terrestrial biosphere model (VECODE) and a
409 phosphate-limited ocean biogeochemical cycle model (Brovkin et al 2002, Brovkin et al 2007,
410 Ganopolski et al 1998).

411 **The GENIE-1 model**

412 The three versions of the Grid ENabled Integrated Earth system model (GENIE-1) employed in
413 this study (GENIE8, GENIE16, MESMO) are all based on the same fast climate model of
414 Edwards and Marsh (2005), which features a reduced physics (frictional geostrophic) 3-D ocean
415 circulation model coupled to a 2-D energy-moisture balance model (EMBM) of the atmosphere
416 and a dynamic-thermodynamic sea-ice model. The ocean model includes a representation of
417 marine carbon cycling parameterizing biogenically induced geochemical fluxes based on a
418 phosphate control of biological productivity, and calibrated against observational datasets of
419 ocean geochemistry (Ridgwell et al., 2007a). The primary differences between the three versions

of GENIE-1 (GENIE8, GENIE16, MESMO) concern the vertical resolution, means of parameter value calibration, and parameter values as described below and listed in Table S1.

GENIE8

'GENIE8' divides the model ocean into 8 vertical levels and has non-seasonal climatology identical to that described in Ridgwell et al. (2007a). Parameter values controlling climate were obtained by means of an ensemble Kalman filter (EnKF) methodology described in Hargreaves et al. (2004), with annual mean climatological observations of ocean salinity and temperature together with surface air temperature and humidity assimilated.

The marine carbon cycle was also calibrated by means of EnKF as described in Ridgwell et al. (2007a), but in addition to assimilating information concerning modern observations of ocean phosphate and alkalinity distributions, experimental observations of *p*H impacts on plankton calcification inform the prior uncertainties for calcification rate power (η) (Ridgwell et al., 2007b).

GENIE16:

'GENIE16' employs a 16 vertical level version of the ocean circulation component, and is forced by seasonal insolation (but annual average wind stress). The climatology of this configuration of GENIE-1 has been calibrated by means of a multi-objective tuning process as described in Matsumoto et al. (2008), using exactly the same observational climatological data as for the EnKF calibration of GENIE8 (Hargreaves et al., 2004) (except at increased vertical resolution in the ocean). Temperature diffusion around Antarctica (90-60°S) is additionally reduced by 75% in the 2-D atmospheric energy balance module to capture some of the relative (seasonal) isolation

441 of the atmosphere in this region. The resulting configuration of the climate model and resulting
442 climatology is identical to that described in Singarayer et al. (2008).

443 The biogeochemical parameters are calibrated by the same multi-objective tuning process
444 described in Matsumoto et al. (2008) and against the same 3-D ocean phosphate and alkalinity
445 data-sets as for GENIE8, but without additional observational constraints on plankton
446 calcification sensitivity (i.e., as per Ridgwell et al., 2007a). In addition, to ensure numerical
447 stability of the calculation of atmosphere-ocean surface gas equilibrium, the time-stepping
448 between ocean biogeochemistry and circulation is reduced to 1:2, compared to the 1:5 ratio used
449 in GENIE8 (Ridgwell et al., 2007a).

450 **MESMO**

451 Derived from GENIE-1 and like GENIE16, MESMO has 16 vertical levels and is forced by
452 seasonal insolation. An important distinguishing feature of MESMO is the use of depth-
453 dependent vertical diffusivity in the ocean. This improves significantly the ventilation of the
454 interior ocean such that the deep ocean $\Delta^{14}C$ as well as the inventories of anthropogenic carbon
455 and CFCs are consistent with data-based estimates. In addition, biological production occurs in
456 the top two layers above the compensation depth of 100m and is modified by additional
457 parameters, such as diagnosed mixed layer depth and temperature. In the steady state control run,
458 the annual export production of POC is 10.6 PgC and of $CaCO_3$ is 1.0 PgC. For the historical
459 run where atmospheric pCO_2 is prescribed to follow the observation, $CaCO_3$ export is reduced to
460 0.9 PgC/yr as a result of anthropogenic carbon lowering the carbonate ion concentration. A
461 detailed description of the MESMO model is given in Matsumoto et al. (2008).

462

463 **HILDA**

464 The High-Latitude Exchange-Interior Diffusion/Advection (HILDA) model is a box
465 advection/diffusion model with transport parameters calibrated to match the ocean distribution of
466 natural and bomb-produced radiocarbon (Siegenthaler and Joos, 1992). Here, the model has been
467 applied in its mixed-layer impulse response form (Joos et al., 1996). The model, in combination
468 with representations of the terrestrial biosphere, has been used for CO_2 projections in the IPCC
469 Second and Third Assessment Report (Joos et al., 2001), in IPCC technical papers, and to
470 calculate Global Warming Potentials for the Kyoto Protocol. The model includes an energy
471 balance formulation and the equilibrium climate sensitivity has been set here to 3.2 K for a
472 nominal CO_2 doubling.

473 **LTCM**

474 The Long-term Carbon Cycle Model (LTCM) is a modified and extended ocean carbon cycle
475 model based on the HILDA box advection/diffusion model of Siegenthaler and Joos (1992). The
476 structure of the physical ocean model is built based upon the HIDAL model, but with some
477 modifications. First, the advection of water from the deep high latitude ocean into low latitude
478 ocean occurs at all depths instead of only at the bottom ocean as in HILDA. Second, unlike the
479 original HILDA model in which vertical diffusivity decreases with ocean depth, vertical
480 diffusivity in LTCM increases with depth following Bryan and Lewis (1979). The values of
481 vertical diffusivity and other ocean transport parameters are calibrated against the recent data-
482 based observations of natural radiocarbon (Key et al., 2004). The implementation of
483 biogeochemical cycling closely follows the OCMIP-2 protocols, but biological carbon uptake is
484 parameterized by the Michaelis-Menton type uptake kinetics instead of by restoring surface
485 phosphate to observations as in OCMIP-2. A 1D sediment column lies at the bottom of each

ocean layer following ocean hypsometry and each column is divided into 10 vertical levels with a total depth of 10cm. The solid component of sediment includes $CaCO_3$ and refractory materials. Dissolved inorganic carbon and alkalinity in the pore water exchange with those of ocean water through diffusion. A parameterization of carbonate and silicate weathering as a function of temperature and CO_2 concentrations are included based on the GEOCARB model of Berner and Kothavala (2001). In addition, an energy balance atmosphere is coupled to the ocean model.

MPI-UW

MPI-UW (Mikolajewicz et al., 2007) consists of a coupled coarse-resolution atmospheric general circulation model ECHAM3 (Roeckner et al., 1992) and an updated version of the Large Scale Geostrophic ocean model (LSG) (Maier-Reimer et al., 1993). The ocean carbon cycle is represented by HAMOCC3 ocean biogeochemistry (Winguth et al., 1994). The land biosphere is simulated using the dynamic vegetation model LPJ (Sitch et al., 2003).

UVic

The University of Victoria Earth System Climate Model (UVic 2.8) model consists of a vertically integrated, energy/moisture balance, atmospheric model with dynamic feedbacks, coupled to a modified version of the MOSES2 land surface model, the MOM2 ocean general circulation model, and a dynamic/thermodynamic sea-ice model (Weaver et al. 2001,Meissner et al. 2003). Ocean carbon is simulated by means of an OCMIP-type inorganic carbon-cycle model and a marine ecosystem model, solving prognostic equations for nutrients, phytoplankton, zooplankton, and detritus (Schmittner et al. 2008). Isopycnal mixing and flux corrected transport were used in the ocean model with diapycnal diffusion specified as a horizontally constant, Bryan-Lewis profile. The only three parameters that have been changed from the default 2.8

configuration are the ocean biology fixed production ratio of carbonate to carbon (changed from 0.02 to 0.018), the e-folding depth for carbonate remineralization (changed from 4500 m to 6500 m) and the scale height for carbon in the atmosphere (changed from 7900 m to 8049 m).

Appendix B: Validation of surface ocean response functions

To test how well ocean response functions derived from 590 PgC emission pulse experiments represent the rate of ocean transport for individual models, we constructed a surface ocean response model following Joos et al. (1996) to simulate historical CO_2 uptake by the ocean. Input to the surface ocean response model are: the prescribed CO_2 concentrations, the relationship between modeled surface DIC and pCO_2 derived from each model's 590 PgC emission pulse simulation, the thickness of top model layer, the rate of air-sea gas exchange, and surface ocean response functions for each model. Oceanic CO_2 uptake simulated by full model runs and the corresponding surface ocean response model runs are compared in Table B1. Close agreement in oceanic carbon uptake is observed between full and response model calculations with the largest difference less than 5%, suggesting that surface ocean response functions essentially capture the overall strength of surface-to-deep ocean transport for the corresponding full models. The discrepancy is mainly due to the fact that the response model does not take into account natural variability of ocean transport and the spatial variability of carbon uptake.

References:

Archer D. 1996. A data-driven model of the global calcite lysocline. Global Biogeochemical Cycles 10: 511-26.

Archer, D., Kheshgi, H., and E. Maier-Reimer, Multiple timescales for neutralization of fossil fuel CO_2, Geophys. Res. Lett. 24(4): 405-408, 1997.

Archer, D., Fate of fossil fuel CO_2 in geologic time J. Geophys. Res. doi: 10.1029/2004JC002625, 2005.

Archer, D., M. Eby, V. Brovkin, A. Ridgwell, L. Cao, U. Mikolajewicz, K. Caldeira, K. Matsumoto, G. Munhoven, A. Montenegro, and K. Tokos, Atmospheric lifetime of fossil-fuel carbon dioxide, Annual reviews of Earth and Planetary Sciences (submitted).

Bala, G., K. Caldeira, A. Mirin, M. Wickett and C. Delire, Multicentury changes to the global climate and carbon cycle: Results from a coupled climate and carbon cycle model. Journal of Climate 18 (21) 4531-4544, 2005.

Berner R., A, Kothavala Z, GEOCARB III: A revised model of atmospheric CO_2 over phanerozoic time. Am. J. Sci. 301: 182-204, 2001.

Broecker W. S. and T. Takahashi, Neutralization of fossil fuel CO_2 by marine calcium carbonate, in The Fate of Fossil Fuel CO2 in the Oceans, edited by N.R. Andersen and A. Malahoff, 213, Plenum Press, New York, 1978.

Broecker W. S., T. H. Peng, G. Ostlund, and M. Stuiver, The distribution of bomb radiocarbon in the ocean, J.Geophys. Res., 90, 6953-6970, 1985.

Broecker, W.S., J. R. Ledwell, T. Takahashi, R. Weiss, L. Merlivat, L. Memery, T.H. Peng, B. Jahne, and K. O. Munnich, Isotopic versus micrometeorlogic ocean CO2 fluxes, J. Geophys. Res., 91, 10,517-10,527, 1986.

557 Brovkin V, J. Bendtsen M. Claussen, A. Ganopolski, C. Kubatzki, and V. Petoukhov, Carbon
558 cycle, vegetation and climate dynamics in the Holocene: Experiments with the CLIMBER-2
559 model. Global Biogeochemical Cycles 16: doi: 10.1029/2001GB001662, 2002.
560
561 Brovkin V, A. Ganopolski, D. Archer, and S., Rahmstorf, Lowering of glacial atmospheric CO2
562 in response to changes in oceanic circulation and marine biogeochemistry.
563 *Paleoceanography* 22, 2007.
564
565 Bryan, K. and L. J. Lewis, A water mass model of the world ocean, J. Geophys. Res., 84, 2503–
566 2518, 1979.

567 Caldeira, K., and M. E. Wickett, Anthropogenic carbon and ocean *p*H, Nature, 425, 365– 365,
568 2003.

569 Cao, L., K. Caldeira, and A. K. Jain, Effects of carbon dioxide and climate change on ocean
570 acidification and carbonate mineral saturation, *Geophys. Res. Lett.*, 34, L05607,
571 doi:10.1029/2006GL028605, 2007.

572 Cao L., A. K. Jain, Learning about the ocean carbon cycle from observational constraints and
573 model simulations of multiple tracers, Climatic Change, 10.1007/s10584-008-9421-1, 2008.

574 Cao, L., and K. Caldeira, Atmospheric CO_2 stabilization and ocean acidification, Geophys. Res. Lett.,
575 doi:10.1029/2008GL035072 (in press), 2008.

576 Chuck A., T. Tyrrell, I. J. Totterdell, and P. M. Holligan, The oceanic response to carbon
577 emissions over the next century: investigations using three ocean carbon cycle models.
578 Tellus, 57B, 70-86, 2005.

579 Cox, P.M., R. A. Betts, C. D. Jones, S. A. Spall, and I. J. Totterdell, Acceleration of global
580 warming due to carbon-cycle feedbacks in a coupled climate model, Nature, 408,184-187,
581 2000.

582 Denman K. L., et al., Coupling between changes in the climate system and biogeochemistry. In:
583 Climate Change 2007: The physical science basis. Contributing of working group I to the
584 Fourth Assessment Report of the Intergovernmental Panel on Climate Change.

585 Doney, S. C, Major challenges confronting marine biogeochemical modeling, Global
586 Biogeochem. Cycles, 13, 705–714, 1999.
587
588 Doney, S. C., et al., Evaluating global ocean carbon models: The importance of realistic physics,
589 Global Biogeochem. Cycles, 18, GB3017, doi:10.1029/2003GB002150, 2004.
590
591 Edwards, N. R. A. J. Willmott, and P. D. Killworth: On the role of topography and wind stress
592 on the stability of the thermohaline circulation. J. Phys. Oceanogr., 28**,** 756–778, 1998.
593
594 Edwards, N. R., and R. Marsh, Uncertainties due to transport-parameter sensitivity in an efficient
595 3-D ocean-climate model**,** Climate Dynamics, 24 (4) 415 – 433, 2005.
596
597 Friedlingstein, P., et al, Climate-carbon cycle feedback analysis: results from the C4MIP model
598 intercomparison. J. Clim., 19, 3337–3353, 2006.
599
600 Ganopolski A, Rahmstorf S, Petoukhov V, Claussen M, Simulation of modern and glacial
601 climates with a coupled global model of intermediate complexity. Nature 371: 323-326,
602 1998.
603
604 Gebbie, G., P. Heimbach, and C. Wunsch, Strategies for nested and eddy-permitting state
605 estimation, J. Geophys. Res., 111, C10073, doi:10.1029/2005JC003094, 2006.
606
607 Goosse, H., Modelling the large-scale behavior of the coupled ocean–sea-ice system, Ph.D. thesis,
608 Universite Catholique de Louvain, Louvain-la-Neuve, Belgium, 231 pp., 1998.
609
610 Goosse, H., and T. Fichefet, Importance of ice-ocean interactions for the global ocean circulation:
611 A model study, J. Geophys. Res., 104, 23,337– 23,355, 1999.
612
613 Gordon, C., C. Cooper, C. A. Senior, H. Banks, J. M. Gregory, T. C. Johns, J. F. B. Mitchell, and
614 R. A. Wood, The simulation of SST, sea ice extents and ocean heat transports in a version of
615 the Hadley Centre coupled model without flux adjustments, Clim. Dyn., 16, 147– 168, 2000.
616

617 Hargreaves, J. C., J. D. Annan, N. R. Edwards, R. Marsh, An efficient climate forecasting
618 method using an intermediate complexity Earth System Model and the ensemble Kalman
619 filter**,** Climate Dynamics*,* 23 (7-8), 745 – 760, 2004.
620
621 Heinze, C., Simulating oceanic CaCO3 export production in the greenhouse, Geophys. Res. Lett.,
622 31, L16308, doi:10.1029/2004GL020613, 2004.
623
624 Intergovernmental Panel on Climatic Change (IPCC) , Third Assessment Report of Working
625 Group III, Mitigation, edited by B. Metz et al., 752 pp., Cambridge Univ. Press, New York,
626 2001.
627
628 Joos, F., Bruno, M., Fink, R. Stocker, T.F., Siegenthaler, U., Le Quéré, C., and Sarmiento, J. L.,
629 An efficient and accurate representation of complex oceanic and biospheric models of
630 anthropogenic carbon uptake, Tellus, 48B, 397-417, 1996.
631
632 Joos, F., and M. Bruno. Pulse response functions are cost-efficient tools to model the link
633 between carbon emissions, atmospheric CO_2 and global warming. Physics and Chemistry of
634 the Earth , 21:471-476, 1996.
635
636 Joos, F., G.-K. Plattner, T. F. Stocker, O. Marchal, and A. Schmittner, Global warming and
637 marine carbon cycle feedbacks on future atmospheric CO_2, Science, 284**,** 464-467, 1999.

638 Joos, F., I. C. Prentice, S. Sitch, R. Meyer, G. Hooss, G.-K. Plattner, S. Gerber, and K.
639 Hasselmann. Global warming feedbacks on terrestrial carbon uptake under the
640 Intergovernmental Panel on Climate Change (IPCC) emission scenarios. Global
641 Biogeochemical Cycles , 15, 891-908, 2001

642 Key, R. M., A. Kozyr, C. L. Sabine, K. Lee, R. Wanninkhof, J. L. Bullister, R. A. Feely, F. J.
643 Millero, C. Mordy, and T.-H. Peng, A global ocean carbon climatology: Results from Global
644 Data Analysis Project (GLODAP), Global Biogeochem. Cycles, 18, GB4031,
645 doi:10.1029/2004GB002247, 2004.
646

647 Kraus, E., and J. Turner, A one-dimensional model of the seasonal thermocline: II, Tellus, 19,
648 98– 105, 1967.
649
650 Lenton, T. M., and C. Britton, Enhanced carbonate and silicate weathering accelerates recovery
651 from fossil fuel CO2 perturbations, Global Biogeochem. Cycles, 20, GB3009,
652 doi:10.1029/2005GB002678, 2006.
653
654 Maier-Reimer, E. and K. Hasselmann. Transport and storage of CO_2 in the ocean - an inorganic
655 ocean - circulation carbon cycle model, Climate Dynamics 2, 63-90, 1987.
656
657 Maier-Reimer, E., Geochemical cycles in an ocean general circulation model: preindustrial
658 tracer distributions, Global Biogeochem. Cycles, 7, 645– 677, 1993.
659
660 Maier-Reimer E., The biological pump in the greenhouse, Global and Planetary change, 8, 13-15,
661 1993.

662 Maier-Reimer, E., U. Mikolajewicz and A. Winguth, Future ocean uptake of CO2: interaction
663 between ocean circulation and biology, Clim. Dyn, 12, 711-721, 1996.

664 Marchal, T. F. Stocker and F. Joos, A latitude-depth, circulation-biogeochemical ocean model
665 for paleoclimate studies: Model development and sensitivities. Tellus, 50B, 290-316,
666 1998.

667 Matsumoto, K., et al., Evaluation of ocean carbon cycle models with data-based metrics,
668 Geophys. Res. Lett., 31, L07303, doi: 10.1029/2003GL018970, 2004.
669
670 Matsumoto, K. S. Tokos, A. Price, and S. J. Cox, First description of the Minnesota Earth
671 System Model for Ocean biogeochemistry (MESMO 1.0), Geoscientific Model
672 Development, 1, 1-15, 2008.
673
674 Meissner, K.J., Weaver, A.J., Matthews, H.D. and P.M. Cox, The role of land-surface dynamics
675 in glacial inception: a study with the UVic Earth System Model, Climate Dynamics, 21:515-
676 537. DOI 10.1007/s00382-0352-2, 2003.
677

678 Mikolajewicz U, M. Groger , E. Maier-Reimer, G. Schurgers, M. Vizcaino, and A. Winguth,
679 Long-term effects of anthropogenic CO_2 emissions simulated with a complex earth system
680 model. Climate Dynamics 28: 599-631, 2007.
681
682 Montenegro, A.,V. Brovkin, M. Eby, D. Archer, and A. J. Weaver, Long term fate of
683 anthropogenic carbon, Geophys. Res. Lett., 34, L19707, doi:10.1029/2007GL030905, 2007.
684
685 Mouchet, A. and L. Francois, Sensitivity of a global ocean carbon cycle model to the circulation and to
686 the fate of organic matter: preliminary results, *Phys.Chem. Earth.*, *21*, 511–516, 1996.
687
688 Müller S. A, F. Joos, N. R. Edwards, T. F., Stocker, Water mass distribution and ventilation
689 time scales in a cost-efficient, three-dimensional ocean model. J Climate 19(21):5479–5499
690 DOI 10.1175/JCLI3911.1, 2006.
691
692 Murnane, R. J., J. L. Sarmiento, and C. Le Quéré, Spatial distribution of air-sea CO_2 fluxes and
693 the interhemispheric transport of carbon by the oceans, Global Biogeochemical Cycles, 13**,**
694 287-305, 1999.

695 Najjar, R. G., et al., Impact of circulation on export production, dissolved organic matter, and
696 dissolved oxygen in the ocean: Results from Phase II of the Ocean Carbon-cycle Model
697 Intercomparison Project (OCMIP-2), Global Biogeochem. Cycles, 21, GB3007,
698 doi:10.1029/2006GB002857, 2007.
699
700 Orr, J. C, Global ocean storage of anthropogenic carbon, 116pp, Inst. Peirre Simon Laplace, Gid-
701 sur-Yvette, France, 2002.

702 Orr, J. C., *et al*, Anthropogenic ocean acidification over the twenty first century and its impact on
703 calcifying organisms, Nature, 437, 681–686, 2005.
704
705 Parekh, P., F. Joos, S. A. Müller, The interplay between aeolian iron fluxes and ligands in
706 controlling carbon dioxide fluctuations during Antarctic warm events, Paleoceanography,
707 doi:10.1029/2007PA001531 (in press), 2008.

Plattner, G. K., F. Joos, T. F. Stocker, and O. Marchal, Feedback mechanisms and sensitivities of ocean carbon uptake under global warming, Tellus, 53B**,** 564-592, 2001.

Plattner, G. K., R. Knutti, F. Joos, T. F. Stocker, W. von Bloh, V. Brovkin, D. Cameron, E. Driesschaert, S. Dutkiewicz, M. Eby, N. R. Edwards, T. Fichefet, J. C. Hargreaves, C. D. Jones, M. F. Loutre, H. D. Matthews, A. Mouchet, S. A. Müller, S. Nawrath, A. Price, A. Sokolov, K. M. Strassmann, and A. J, Weaver. Long-term climate commitments projected with climate - carbon cycle models, Journal of Climate, 21, 2721-2751, 2008.

Riebesell et al., Enhanced biological carbon consumption in a high CO2 ocean. Nature, 450, 545-548, 2007.

Ridgwell, A**.**, I. Zondervan, J. Hargreaves, J. Bijma, and T. Lenton, Assessing the potential long-term increase of oceanic fossil fuel CO_2 uptake due to 'CO_2-calcification feedback', Biogeosciences 4, 481-492, 2007a.

Ridgwell, A., J. Hargreaves, N. Edwards, J. Annan, T. Lenton, R. Marsh, A. Yool, and A. Watson, Marine geochemical data assimilation in an efficient Earth System Model of global biogeochemical cycling, Biogeosciences 4, 87-104, 2007b.

Ridgwell, A., and J. C. Hargreaves, Regulation of atmospheric CO_2 by deep-sea sediments in an Earth system model, Global Biogeochem. Cycles, 21, GB2008, doi:10.1029/2006GB002764, 2007.

Roeckner E, K. Arpe, L. Bengtsson , S. Brinkop, L. Duemenil, et al., Simulation of the present-day climate with the ECHAM model: impact of the model physics and resolution. Report No 93., Hamburg, 1992.

Royal Society, "Ocean acidification due to increasing atmospheric carbon dioxide", The Royal society; London, 2005.

Sabine, C. L., et al., The Oceanic Sink for Atmospheric Carbon. Science 305, 367–371, 2004.

Sarmiento, J. L., Orr, J. C. and U. Siegenthaler, A perturbation simulation of CO_2 uptake in an ocean general circulation modeL *J. Geophys. Res. 97,* 3621-3645, 1992.

736
737 Sarmiento, J. L., T. M. C. Hughes, R. J. Stouffer and S. Manabe, Simulated response of the
738 ocean to anthropogenic climate warming, Nature. 393, 245–249, 1998.

739 Schlitzer, R., An adjoint model for the determination of the mean oceanic circulation, air-sea
740 fluxes and mixing coefficients, Ber. zur Polarforschung 156, Alfred-Wegener-Institut,
741 Bremerhaven, 1995.

742
743 Schlitzer, R., Carbon export in the Southern Ocean: Results from inverse modeling and
744 comparison with satellite-based estimates, Deep Sea Res., Part II, 49, 1623–1644, 2002.

745
746 Schmittner, A., A. Oschlies, X. Giraud, M. Eby, and H. L. Simmons, A global model of the
747 marine ecosystem for long-term simulations: Sensitivity to ocean mixing, buoyancy forcing,
748 particle sinking, and dissolved organic matter cycling, Global Biogeochem. Cycles, 19,
749 GB3004, doi:10.1029/2004GB002283, 2005.

750
751 Schmittner A., A. Oschlies, H. D. Matthews and E. D. Galbraith, Future changes in climate,
752 ocean circulation, ecosystems and biogeochemical cycling simulated for a business-as-
753 usual CO_2 emission scenario until year 4000 AD, Global Biogeochem. Cycles, 22,
754 GB1013, doi:10.1029/2007GB00295, 2008.

755
756 Shaffer G, Sarmiento, J. L., Biogeochemical Cycling in the Global Ocean .1. A New, Analytical
757 Model with Continuous Vertical Resolution and High-Latitude Dynamics. J. of Geophy.
758 Res. 100: 2659-72, 1995.

759
760 Siegenthaler, U. and H. Oeschger, Biospheric CO_2 emissions during the past 200 years
761 reconstructed by deconvolution of ice core data, Tellus, 39B, 140–154, 1987.

762
763 Siegenthaler, U. and F. Joos, Use of a simple model for studying oceanic tracer distributions and
764 the global carbon cycle. *Tellus* 44B, 186-207, 1992.

765
766 Singarayer J. S., D. A. Richards, A. Ridgwell, P. J. Valdes, W. E. N. Austin, J. W. Beck, An
767 oceanic origin for the increase of atmospheric radiocarbon during the Younger Dryas,
768 Geophys. Res. Lett. 35, L14707, doi:10.1029/2008GL034074, 2008.

769 Steinacher, M. F. Joos, T. L. Frölicher, G.-K. Plattner, and S. C. Doney, Ocean acidification in
770 the Arctic projected with the NCAR global coupled carbon cycle-climate model,
771 Biogeoscience, (submitted), 2008.
772
773 Stocker, T. F., D. G. Wright, and L. A. Mysak , A zonally averaged, coupled ocean-atmosphere
774 model for paleoclimate studies, J. Clim., 5, 773–797, 1992.
775 Tschumi, T., F. Joos, P. Parekh, How important are Southern Hemisphere wind changes for low
776 glacial carbon dioxide? A model study, Paleoceanography, DOI:10.1029/2008PA001592,
777 2008 (in press).
778
779 Walker, J. C. G., and J. F. Kasting, Effects of fuel and forest conservation on future levels of
780 atmospheric carbon dioxide, Palaeogeog, Palaeoclimatol., Palaeoecol., 97, 151-189, 1992.

781 Waugh D. W., T.M. Hall, B. I. Mcneil, R. Key, and R. J. Matear, Anthropogenic CO_2 in the
782 oceans estimated using transient time distributions, Tellus 58B, 376-389, 2006.

783 Weaver, A. J., et al., The UVic Earth System Climate Model: Model description, climatology
784 and application to past, present and future climates, Atmos-Ocean, 38**,** 271–301, 2001.

785 Willey, D. A., R. A. Fine, R. E. Sonnerup, J. L. Bullister, W. M. Smethie Jr., and M. J. Warner,
786 Global oceanic chlorofluorocarbon inventory, Geophys. Res. Lett., 31, L01303,
787 doi:10.1029/2003GL018816, 2004.
788
789 Winguth A., M., Heimann K. D. Kurz, E. Maier-Reimer, U. Michajewicz, and J. Segschneider,
790 ENSO related fluctuations of the marine carbon cycle. Global Biogeochem. Cycles 8: 39-65,
791 1994.
792
793 Wright, D. G. and T. F. Stocker, Sensitivities of a zonally averaged global ocean circulation
794 model, J. Geophys. Res., 97, 12707–12730, 1992.
795
796 Wright, D. G. and T. F. Stocker, Closures used in zonally averaged ocean models, J. Phys. Oceanogr., *28*,
797 701–804, 1998.
798

799 Yamanaka, Y., and E. Tajika, The role of the vertical fluxes of particulate organic matter and
800 calcite in the oceanic carbon cycle: Studies using an ocean biogeochemical circulation
801 model, Global Biogeochem. Cycles, 10, 361– 382, 1996.
802
803 Zeebe, R. E.**,** and K. Caldeira, Close mass balance of long-term carbon fluxes from ice-core CO_2
804 and ocean chemistry records. Nature Geoscience, doi:10.1038/ngeo185, 2008.
805
806 Zickfeld, K., J. C. Fyfe, O.A. Saenko, M. Eby, and A. J. Weaver, Response of the global carbon
807 cycle to human-induced changes in Southern Hemisphere winds, Geophys. Res. Lett, 34,
808 L12712, doi: 10.1029/2006GL028797, 2007.

Table 1. Key features of models used in this study

	Horizontal resolution (Lon × Lat)	Vertical levels	Top layer thickness (m)	Surface forcing	Seasonality	Lateral mixing	Vertical diffusivity ($cm^{-2}\ s^{-1}$)[%]	Mixed layer scheme	Sea ice
AWI	5° × 4° to 2.5° × 2°	26	61	adjusted	no	ISOP	0.1	-	no
Bern2.5D[#]	10° - 15° × basin average	14	50	EMBM	no	HOR	0.4	-	yes
Bern3D	10° × 3.2° to 19.2°	32	38.9	flux, restoring	yes	ISOP, GM	0.1	-	no
GENIE8	10° × 3.2° to 19.2°	8	174.8	EMBM	no	ISOP,GM	0.27	-	yes
GENIE16	10° × 3.2° to 19.2°	16	80.8	EMBM	yes	ISOP,GM	0.25	-	yes
HILDA	high and low latitude boxes	69	75	EMBM	no	-	0.15-2.4	-	no
IGCR*	4° × 4°	66	50	restoring	no	HOR	0.3	-	no
LTCM	high and low latitude boxes	37	75	EMBM	no	-	1.3-9.7	-	no
MESMO	10° × 3.2° to 19.2°	16	45	EMBM	yes	ISOP, GM	0.1-1.2	-	yes
MPI-UW	5.6° × 5.6°	22	50	AGCM	yes	ISOP, GM	0.1-V_{max}[&]	-	yes
SOC	2.5° × 3.75°	20	10	flux, restoring	yes	ISOP, GM	0.1-1.5	KT	no
UL	3° × 3°	20	10	bulk formula	yes	HOR	0.1-1.1	TKE	yes
UVic	3.6° × 1.8°	19	50	EMBM	yes	ISOP, GM	0.3-1.3	-	yes

Abbreviations are as follows: EMBM: Energy and moisture Balance Model; HOR: Horizontal mixing parameterization; ISOP: Isopycnal mixing parameterization; GM: Gent and McWilliams (1990) mixing parameterization; KT: Kraus and Turner (1967) parameterization; TKE: Turbulent Kinetic Energy closure; AGCM: atmosphere general circulation model.

* It is now recognized as FRCGC (Frontier Research Center for Global Change)

[#] Previously known as PIUB

[%] Vertical diffusivity decreases with depth in HILDA, while increase with depth for other models with a depth-dependent profile

[&] A single maximum vertical diffusivity for MPI-UW (V_{max}) is not available, which depends on wind speed and stratification

Key references for each model are: AWI, Schiltzer (2002); IGCR, Yamanaka and Tajika (1996); Bern2.5D, Stocker et al. (1992); Bern- 3D, Müller et al. (2006); SOC, Gordon et al., (2000); UL, Goosse and Fichefet (1999); UVic, Weaver et al. (2001); GENIE8: Ridgwell et al., 2007a GENIE16, Singarayer et al. (2008); MESMO, Matsumoto et al. (2008); MPI-UW, Mikolajewicz et al. (2007); HILDA, Siegenthaler and Joos (1992).

Table B1. Historical CO_2 uptake (PgC) simulated by full model runs and corresponding surface ocean response model runs. A 3% downward correction is applied to the 1990s CO_2 uptake for AWI, Bern2.5D, and IGCR (Orr et al., 2002), which are from simulations using the IPCC S650 scenario with 1990s atmospheric CO_2 concentrations slightly higher than the observed.

	1980-1999		1765-2000	
	full model	response model	full model	response model
AWI	46.4	44.7	160.0	159.0
IGCR	44.5	43.6	149.1	151.2
Bern2.5D	46.3	45.5	155.5	155.1
Bern3D	36.2	35.8	123.5	120.0
UVic	39.2	37.1	135.3	130.3
GENIE8	56.5	56.1	187.9	184.0
GENIE16	40.1	38.6	134.1	132.9
LTCM	37.2	37.5	121.1	122.2

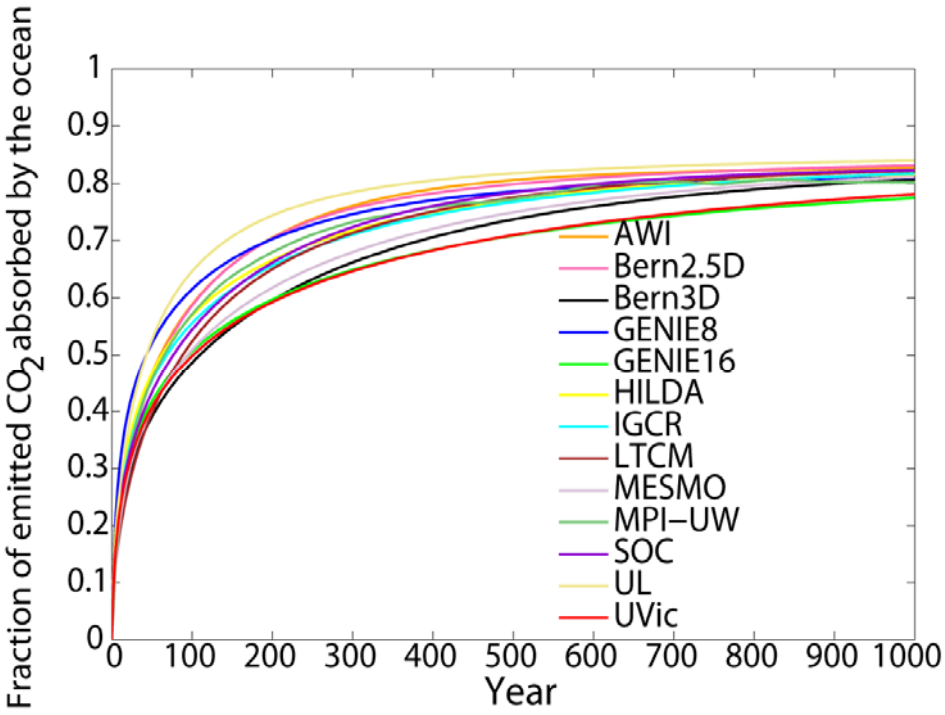

Figure 1. Model-simulated oceanic uptake of CO_2 in response to a CO_2 pulse emission of 590.2 PgC (corresponding to an instantaneous doubling of atmospheric CO_2 from 278 to 556 ppm)

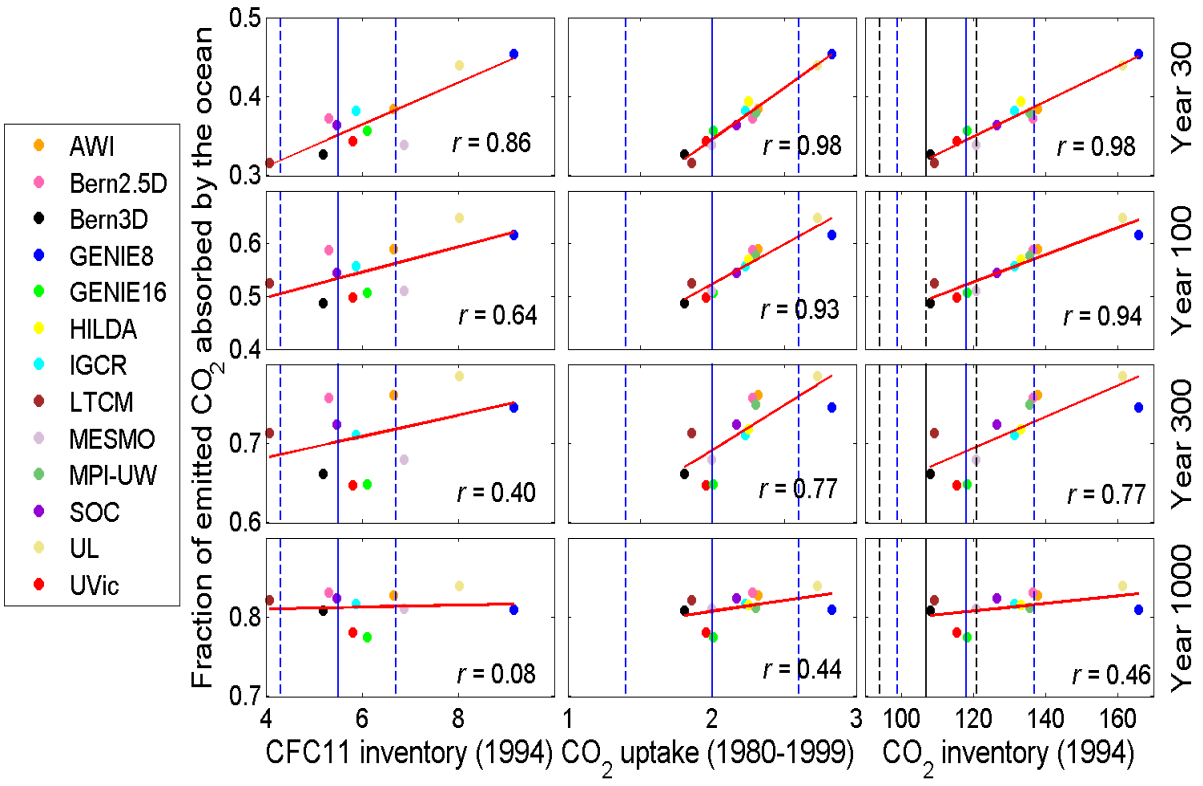

Figure 2. Correlation of the oceanic uptake for anthropogenic CO_2 in response to an emission pulse of 590.2 PgC with model-simulated CFC11 inventories (10^8 mole) in year 1994, mean anthropogenic CO_2 uptake (PgC/yr) between year 1980 and 1999, and anthropogenic CO_2 inventories (PgC) between year 1800 and 1994 (A 3% downward correction is applied to the 1990s CO_2 results for AWI, Bern2.5D, IGCR, PIUB, SOC, and UL (Orr et al., 2002), which are from simulations using the IPCC S650 scenario with 1990s atmospheric CO_2 concentrations slightly higher than the observed). The results are shown for years 30, 100, 300, and 1000 (following logarithmic distributions) after emission pulse. Vertical lines in each panel represent observational data (solid lines) and associated uncertainties (dashed lines). Observed CFC11 inventory is from Willey et al. (2004), CO_2 uptake is from Denman et al (2007), and CO_2 inventory is from Sabine et al. (2004) (blue lines) and Waugh et al. (2006) (black lines). Also shown in each panel is the trend line and correlation coefficient. Model results shown here did not include climate feedbacks. If climate feedbacks are included, uptake and inventories are slightly lower. Simulations of CFCs were not performed by MPI-UW and HILDA.

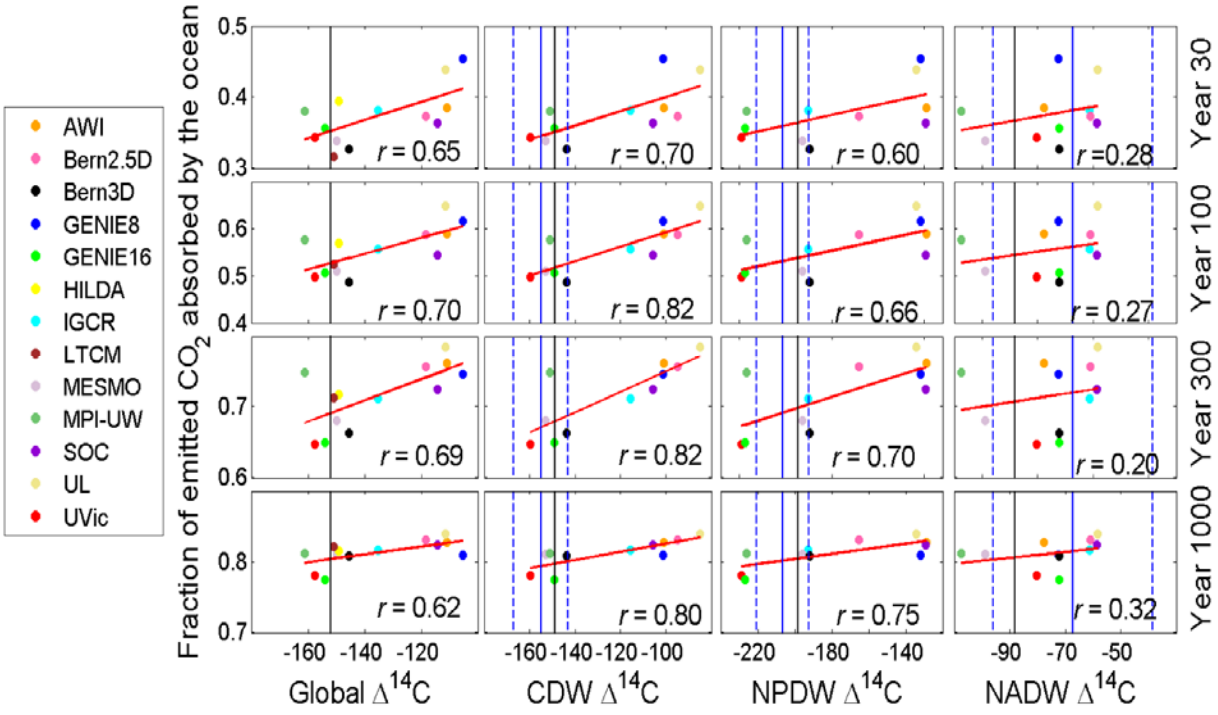

Figure 3. Correlation of the oceanic uptake for anthropogenic CO_2 in response to an emission pulse of 590.2 PgC with natural radiocarbon (permil) of the global ocean, Circumpolar Deep Water (CDW, 90-45ºS, 1500-5000 m), North Pacific Deep Water (NPDW, Equator-60ºN, 1500-5000 m), and North Atlantic Deep Water (NADW, Equator-60ºN, 1000-3500 m). The results are shown for years 30, 100, 300, and 1000 (following logarithmic distributions) after emission pulse. Vertical lines in each panel represent observational data (solid lines) from Global Data Analysis Project (GLODAP) (Key et al., 2004) and associated uncertainties (one standard deviation, dashed lines). Analysis of Matsumoto et al. (2004) using the GLODAP bottle data is represented by blue lines, and our analysis using regridded GLODAP data are represented by black lines. Also shown in each panel is the trend line and correlation coefficient *r*.

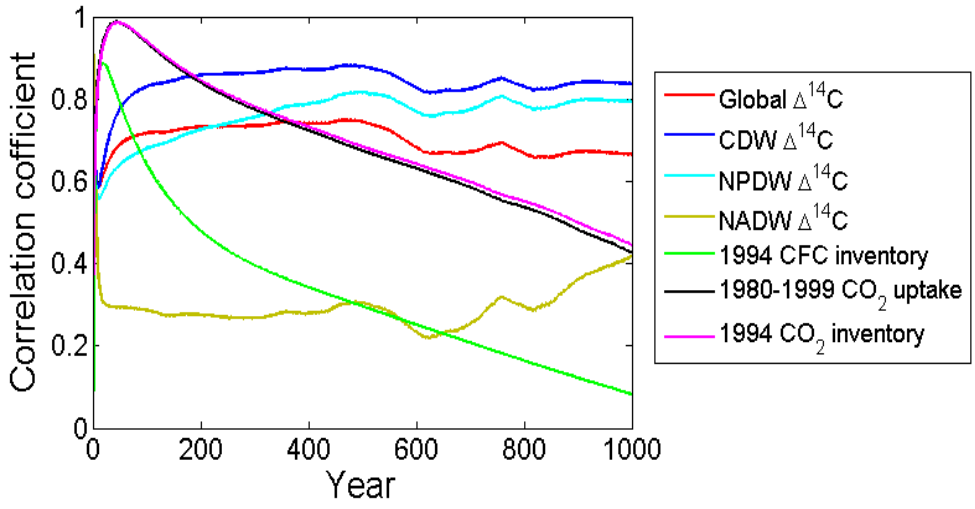

Figure 4 Correlation of the oceanic uptake for anthropogenic CO_2 in response to an emission pulse of 590.2 PgC with simulated natural $\Delta^{14}C$, CFC inventory (10^8 mole), CO_2 inventory (PgC), and CO_2 uptake (PgC/yr). On timescales from decades to a few centuries, modeled oceanic absorption of CO_2 emitted is strongly correlated with present-day uptake and inventory of anthropogenic CO_2. On timescales from a century to a millennium, the amount of CO_2 released absorbed by the ocean is strongly correlated with the content of natural radiocarbon in the deep Southern and Pacific ocean. CDW: Circumpolar Deep Water (90-45ºS, 1500-5000 m); NPDW: North Pacific Deep Water (Equator-60ºN, 1500-5000 m); NADW: North Atlantic Deep Water (Equator-60ºN, 1000-3500 m).

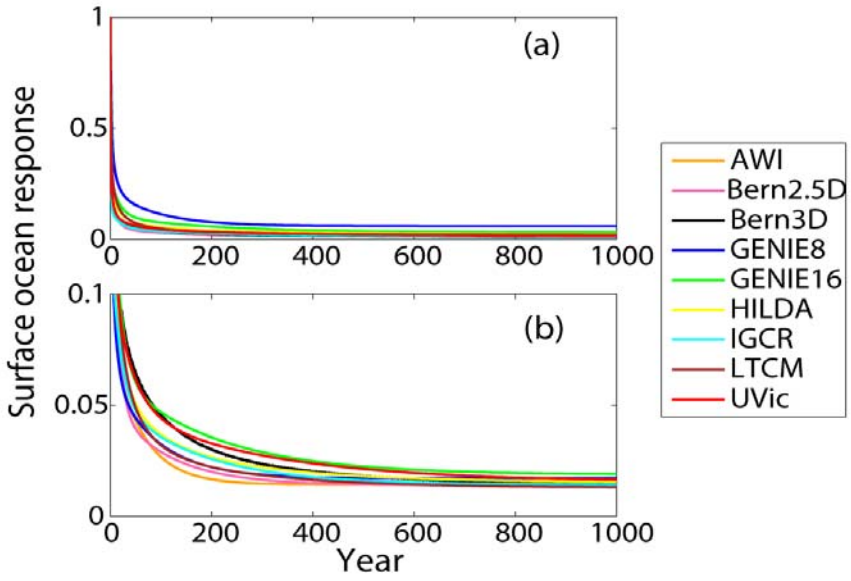

Figure 5. Ocean surface responses that represent the fraction of an initially added amount of tracer to the surface ocean that remains in the surface after a certain time (a) ocean surface responses determined from the 590.2 PgC CO_2 emission pulse experiments for individual models; (b) The same responses as (a), but normalized by a uniform surface depth of 50 m by multiplying each response by 50 m and divided by the top layer thickness of each model. Note that different scales are used in (a) and (b).

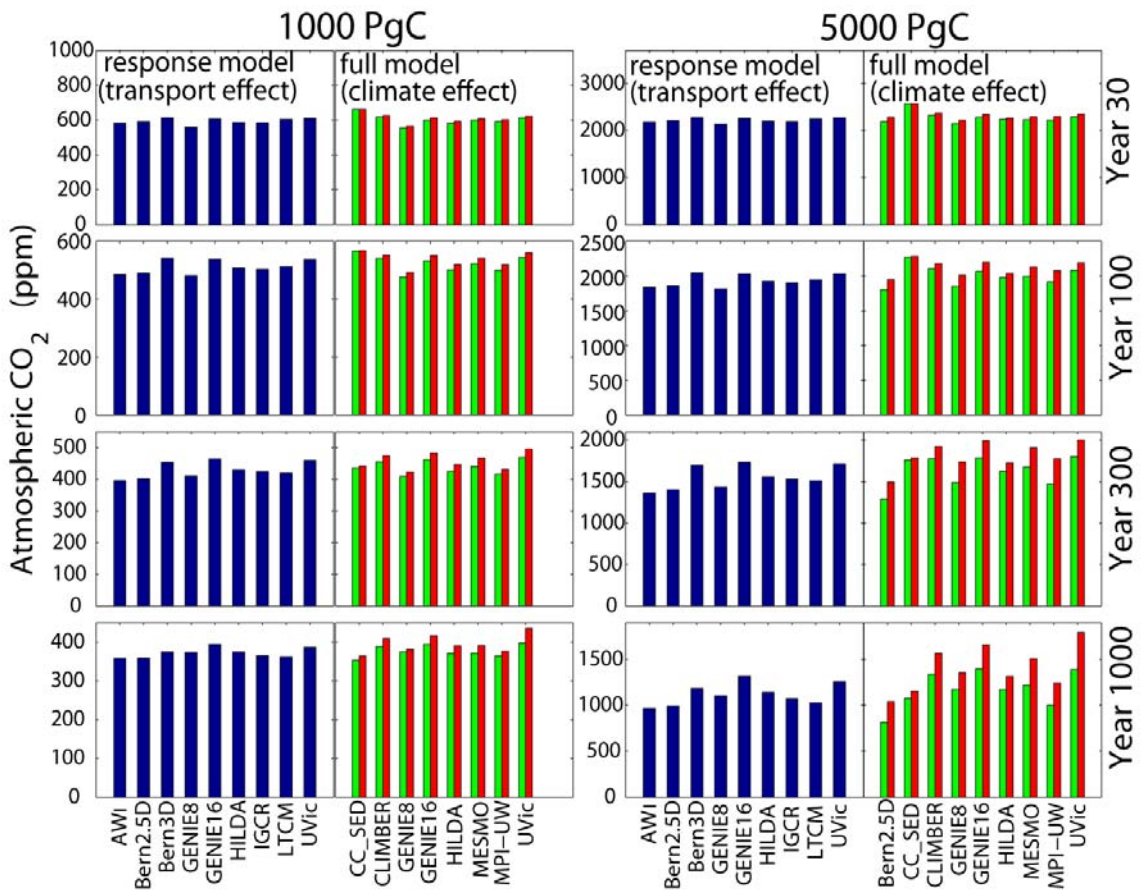

Figure 6. Projected atmospheric CO_2 concentrations (by assuming a neutral terrestrial biosphere) in response to 1000 and 5000 PgC emission pulses using surface ocean response model (dark blue bars) and full model runs with the inclusion of climate feedbacks on the ocean carbon cycle (red bars) and without it (green bars). The differences in CO_2 concentrations calculated by ocean response model runs are a result of differences in the rate of surface-to-deep ocean transport across models, while the differences in CO_2 concentrations calculated by full model runs are a result of climate feedbacks on the ocean carbon cycle in a single model associated with changes in temperature, circulation, and marine biology. It is shown that the effect of different ocean transport across models on projected atmospheric CO_2 concentrations is comparable to that of climate change in a single model (by assuming a neutral terrestrial biosphere).